IOP PUBLISHING JOURNAL OF PHYSICS D: APPLIED PHYSICS

J. Phys. D: Appl. Phys. **42** (2009) 165204 (9pp) doi:10.1088/0022-3727/42/16/165204

Human dermis separation via ultra-short pulsed laser plasma-mediated ablation

Huan Huang and Zhixiong Guo[1]

Department of Mechanical and Aerospace Engineering, Rutgers, The State University of New Jersey, Piscataway, NJ 08854, USA

E-mail: guo@jove.rutgers.edu

Received 20 April 2009, in final form 9 June 2009
Published 31 July 2009
Online at stacks.iop.org/JPhysD/42/165204

Abstract

In vitro layer separation of human dermal tissues via laser plasma-mediated ablation was successfully conducted for the first time. The ablation of wet dermis was generated using a 900 fs ultra-short pulsed laser with the wavelength centred at 1552 nm. The ablation and separation results were imaged and measured by scanning electron microscopy. The dermis ablation threshold was determined as $9.65 \pm 1.21\,\mathrm{J\,cm^{-2}}$ and the incubation factor was found as 0.46 ± 0.03. Histological examinations were performed to find proper laser parameters for dermis ablation and separation with minimal thermal damage. No thermal damage was found in the single line ablation results when the pulse overlap rate was not over 5 pulses $\mu\mathrm{m}^{-1}$. Even in the multi-line ablation, thermal damage was insignificant and the lateral damage zone was generally within 5 μm in the results with 100 continuously repeated line scans. The separation of a whole piece of wet dermal tissue into two thin layers was presented. Several separation tests with different layer thicknesses from 200 to 600 μm were completed. The unevenness of the separated layers was generally under 10%. The cohesion and morphology of the separated tissue layers were not altered.

(Some figures in this article are in colour only in the electronic version)

1. Introduction

Skin grafting originated approximately 2500 to 3000 years ago and has evolved over the last century into an option that is routinely and sometimes preferentially used during soft tissue reconstruction. The number of patients recovering from post-burn and post-traumatosis by graft tissue implantation is growing. Nowadays in the USA over 900 000 allografts are transplanted each year.

Naturally derived materials such as allograft, xenograft and autograft tissues have many biological, chemical and mechanical advantages over synthetic materials, and thus hold tremendous potential for use in tissue transplantation and therapies. However, surgical treatment is frequently restricted by the scarcity of adequate tissues available for reconstruction. Separation of a tissue into two or multiple layers leads to augmented usages of the limited tissues, doubling or even tripling the harvest of donor tissues. Moreover, a tissue may have to be separated into layers, as the tissue in its entirety may not be necessary or appropriate for implantation [1]. In the treatment of burn wounds, for instance, in many cases it is necessary only to implant the epidermal layer of a skin allograft [2]. It is also known that in many cases only an acellular dermis is needed for facial soft tissue augmentation [3] or for breast reconstruction [4].

The use of these natural biomaterials typically requires chemical or physical pretreatment for sterilization and immunogenicity reduction and other processing, such as preparing the tissue by cutting and shaping the tissue into an appropriate form before transplanting it into a patient or subject [1–5]. However, effective and efficient methods are lacking for separating natural tissues into thin layers and for precisely cutting and shaping tissues without collateral damage [1], according to experts in the Musculoskeletal Transplant Foundation (MTF), the largest tissue bank in the USA. Techniques using a mechanical tool or surgical knife to separate a tissue into multiple layers or to cut the tissue into portions are often limited in precision, resulting in a large amount of waste. It is noted that those mechanical tools can

[1] Author to whom any correspondence should be addressed.

cause damage to the underlying layers and surrounding tissues in the range of 0.1 to 1 mm. For the chemical method, it is time consuming and the residues at the tissue sample could be hard to remove and harmful for the safety of further usage. Thus, it would be very useful to develop an effective method that can precisely and non-intrusively modify tissues with minimized damage.

Lasers have become irreplaceable tools in modern medicine, spanning a wide spectrum of applications from laser surgery [6] to optical imaging [7]. Laser ablation, which has the great advantage of precise material removal, is a promising method in processing and treatment of biological tissues [8–11], biodegradable polymers [12–14], collagen gels [15], dental implants [16], etc. At a low laser flux, the material is heated by the absorbed laser energy and evaporates or sublimates. At a high laser flux, the material is typically converted to plasmas. One describes the effect as a strong local ionization of the medium, where the plasma reaches a density beyond the critical value. Energy is very efficiently absorbed, and the local plasma temperature increases dramatically. An explosive Coulombian expansion producing cavitation follows and forms a very powerful and damaging shockwave that develops on a nanosecond timescale. If the rate of plasma formation is relatively slow, in the nanosecond time regime (for nanosecond excitation laser pulses) or longer, energy is transferred from the plasma to the lattice, and thermal damages like melting or charring of the surrounding tissue can occur.

In the ultrafast time regime (for femto- or picosecond pulses produced by ultra-short pulsed (USP) lasers) the plasma expansion happens on a timescale smaller than the rate of energy transfer to the lattice, and thermal damages are reduced or eliminated [11, 14]. The so-called plasma-mediated ablation occurs when the incident energy flux is over the threshold for optical breakdown ($>10^{11}$ W cm^{-2} in liquids and solids). Furthermore, the substantial plasma generation and absorption enable the ablation of materials that are normally difficult to ablate by continuous wave or nanosecond pulsed lasers, such as transparent or low absorption materials [12–14]. Thus, efficient processing of almost all tissue types via the USP laser plasma-mediated ablation is possible. These distinct features make USP lasers very useful as a promising tool for separating or cutting tissues. In a recent work [14], the present authors have demonstrated clean and clear separation and fabrication of polydimethylsiloxane (PDMS) thin layers and networks without collateral damage via the USP laser plasma-mediated ablation.

In this paper, investigations were extended to fundamentals of USP laser ablation of human dermis and application to *in vitro* tissue separation or cutting. First, parametric studies were conducted to characterize the USP laser plasma-mediated ablation at wet dermis surfaces. The ablation line features as well as the ablation threshold and incubation factor were analysed. The ablation widths and depths resulting from different laser parameters were compared. Then histological views of the ablated wet dermis samples were presented to examine the degree of thermal damage. The objective is to find proper laser parameters that will result in minimal collateral damage for dermis ablation and separation. Finally, separation of dermis layers was demonstrated and the layer uniformity was inspected with several different tests.

2. Methods and materials

2.1. Experimental setup

The experimental setup for USP laser tissue ablation is composed of four main parts: a USP laser, a beam delivery system, a work stage and a whole control system. A commercial erbium doped fibre laser (Raydiance, Inc.) was used in the instrumentation. The laser outputs pulses with a repetition rate tunable between 1 Hz and 500 kHz. The output pulse energy is variable from 1 to 5 μJ. The laser central wavelength is 1552 nm and its pulse width is 900 fs. In the beam delivery system, the laser beam was focused onto the target through an objective lens (Mitutoyo M Plan Apo NIR 20×, NA = 0.40, $f_{\mathrm{L}} = 20$ mm) as shown in figure 1. The laser beam before the lens is about 10 mm in diameter and the diffraction-limit focal spot diameter ($2.44\lambda f_{\mathrm{L}}/D$) in free space is estimated as 8 μm. A digital power meter was used to measure the laser power loss in the beam delivery system. It is found that the total loss is about 50%. Such a loss has been accounted for in the irradiation pulse energy values stated hereafter.

The whole control system is a RayOS™ laptop interface which controls the laser output parameters (mainly pulse energy and repetition rate) as well as the motion of the three-axis precision compact linear stage (VP-25XA, Newport). The work stage for mounting a tissue sample was fixed to the 3D automated translation stage through which the alignment of optics and laser scanning were realized. There are two designs for the work stage in this study. Figure 1(*a*) shows the schematic diagram of experimental setup I with a plate fixture for sample mounting. This setup is simple and was used for characterizing the single line scanning ablation features.

To separate a piece of dermis into two layers, it requires tens of thousands of ablation lines and the process is very time consuming. A wet tissue mounting on the simple plate fixture was apt to dehydrate and deform because of the stage movement. In order to avoid the deformation, a moisture chamber that keeps the tissue wet during the laser processing was utilized as sketched in figure 1(*b*). A tissue feeding and pulling scheme was also designed in experimental setup II as shown in figure 1(*b*) such that the separation interface was always exposed to the laser focal spot through the pulling of two opposite tension forces. Therefore, one does not have to focus the beam into deep tissue and the strong attenuation of biological tissues against light was not a concern. With laser ablation at the exposed interface, the two opposite tension forces pull and split the dermis into two separate layers. An evacuator system (FX225, EDSYN) which is not shown in figure 1 was also employed to collect the plasma plume residue and debris during the laser processing.

2.2. Tissue samples

In this study, donor dermal tissues were used. The wet human dermis samples were prepared and provided by professionals

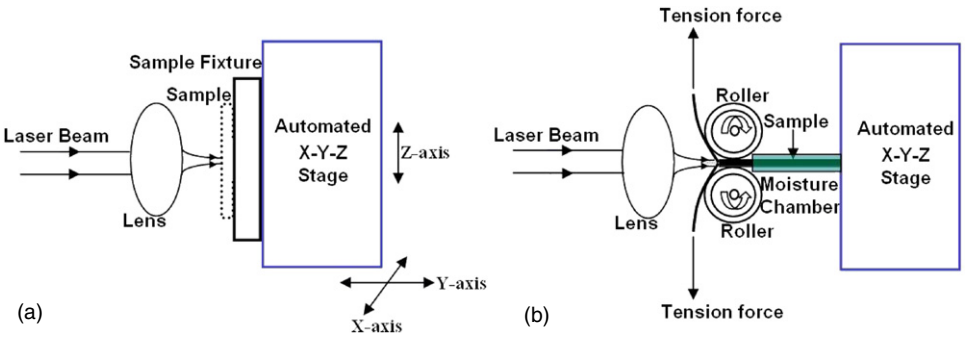

Figure 1. (*a*) Experimental setup I for single line ablation and (*b*) experimental setup II for multi-line ablation and separation.

from the project sponsor, MTF. The donor skin tissue was processed with a series of soak processing—sodium chloride, triton and finally disinfection soak to get the epidermis removed and the processed wet tissue sample was whole dermis. The dermal tissue samples were about 2 mm thick and precut into dimensions of about 10 mm length and 5 mm width, if not otherwise specified.

Like most natural objects the human skins have spectral variability, which in this case is mainly due to amount, density and distribution of melanin. The skin can be described as an optically inhomogeneous material because under the surface there are colourant particles which interact with light, producing scattering and colouration. It is well known that light scattering in biological tissues is very strong [17]. At a wavelength of 1552 nm, water absorption in wet dermis is also significant; and this may reduce the effect of scattering and improve ablation quality [18].

2.3. Microscopy and measurements

Immediately following the ablation experiment, the micro topography and surface quality of the ablated tissue sample were examined by an upright digital microscope (National Optical DC3-156-S). Then the treated samples were fixed in 2% phosphate buffered glutaraldehyde for 2 h, rinsed twice in a phosphate buffer and dehydrated in ethanol. After critical point drying and metal coating, the tissue samples were checked by scanning electron microscopy (SEM) (AMRAY 1830I). For the histological evaluation, the samples were routinely dehydrated in a series of graded ethanol. Then the samples were fixed in paraffin wax and sectioned into 10 μm-thick slices. After that, the slices were stained with hematoxylin and eosin (H&E). Finally the samples were viewed and photographed by a Nikon Eclipse E600 microscope system. The thickness of the separated samples was measured by a vernier caliper.

3. Results and discussion

3.1. Line scanning and ablation threshold

To enable practical tissue separation, ablation features of surface line scanning and the ablation threshold of the wet human dermis must first be understood. The main parameters that affect the ablation include irradiation pulse energy, pulse repetition rate and speed of scanning. The irradiation pulse energy, E, which is 50% of the laser output energy, determines whether the incident laser fluence is above the critical value that plasma-mediated ablation occurs. The pulse repetition rate, f, and the moving speed of work stage, s, determine the pulse overlap intensity and can be combined into one parameter—the pulse overlap rate which is equal to f/s.

Multiple wet dermis samples have been chosen to study line scanning features on the sample surface with different laser parameters. After irradiation, inspections of the ablation lines and measurements of ablation line features are conducted by the SEM. Figure 2 shows four representative SEM images for the four ablation lines generated with irradiation pulse energy 1.0–2.5 μJ, respectively. The pulse repetition rate was 500 kHz and the moving speed of the stage was 25 mm s^{-1}. Thus, the pulse overlap rate was 20 pulses μm^{-1}. From the SEM top view images such as figures 2(*a*) and (*b*), one can measure the average ablation line width as 18.5$\pm$1.3 μm and 15.6$\pm$0.7 μm for the cases of 2.5 μJ and 2.0 μJ irradiation pulse energies, respectively. The standard deviation is based on three different ablated samples. The cut width using mechanical tools such as general surgical blade or scalpel is in the range from 100 μm to 1 mm [1]; so the USP laser ablation is more precise and results in less waste. Figures 2(*c*) and (*d*) are representative views with a tilt angle for the ablation lines of 1.5 μJ and 1.0 μJ irradiation pulse energies, respectively. It is seen that the dermis surface is not very flat and has a roughness of about 5 μm. This roughness will certainly enhance light scattering on the surface and affect the effective size of the beam focal spot at the dermis surface.

For laser pulses with a Gaussian spatial beam profile, the feature size obtained is related to the maximum laser fluence, F_0, on the samples' surface. In laser ablation, the effective radius, r_{eff}, of the focal spot can be found by the slope of the following formula [19]:

$$D^2 = 2r_{\mathrm{eff}}^2 \ln\left(\frac{F_0}{F_{\mathrm{th}}}\right), \tag{1}$$

where D is the diameter of the ablation crater and F_{th} is the ablation threshold fluence. For laser pulses with a Gaussian spatial beam profile, the maximum irradiation fluence F_0 can be calculated from the irradiation pulse energy E as

$$F_0 = \frac{2E}{\pi r_{\mathrm{eff}}^2}. \tag{2}$$

An ablation line consists of continuously ablated craters along the laser scanning direction. When the pulse overlap rate is so

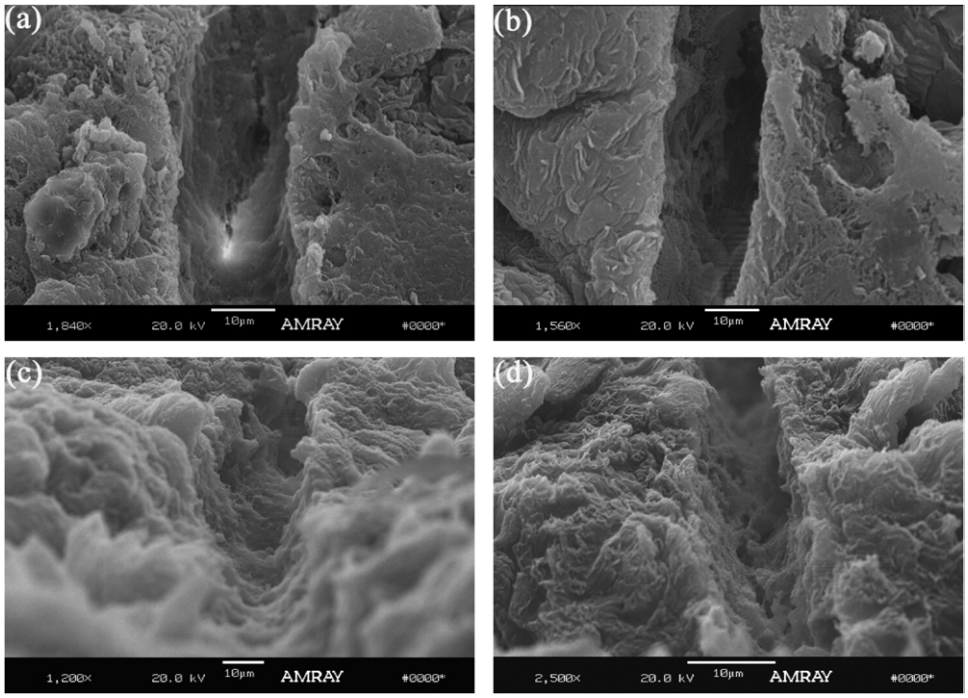

Figure 2. SEM images of the single line ablations with a fixed pulse overlap rate of 20 pulses μm^{-1} and different irradiation energies: (*a*) 2.5 μJ, (*b*) 2.0 μJ, (*c*) 1.5 μJ and (*d*) 1.0 μJ.

intense that no individual crater can be distinguished (such as displayed in figure 2), the ablation line width is then equivalent to the diameter of the ablated crater generated by N repeated pulses. The equivalent pulse number can be approximated by

$$N = 2r_{\text{eff}} f/s. \tag{3}$$

Figure 3 plots the relationship of the square of the ablation line width versus the logarithm of irradiation pulse energy for three different pulse overlap rates. As pointed out by Bonse *et al* [20], the data at high fluence points should be excluded from linear fitting because the deviation of the intensity from the Gaussian distribution at the 'edge' of the high fluence beam will lead to nonlinearity. It should be mentioned that the accumulated fluence for the present ablation lines is very high because the equivalent pulse number N is very large as calculated in table 1. Thus, only low fluence points are adopted for the linear fitting to obtain the slopes of the three curves in figure 3, in particular for the curve with 20 pulses μm^{-1} pulse overlap rate. The calculated effective radii for the focal spots with different pulse overlap rates and the corresponding equivalent pulse numbers are listed in table 1. It is seen that the effective spot size (9–17 μm) is bigger than the diffraction-limit spot size (8 μm) in free space. This is consistent with the results of Mullan *et al* [21] and Choi *et al* [22] for polymers and can be attributed to the strong scattering of light on the rough dermis surface. When the pulse overlap rate is just 5 pulses μm^{-1}, it is seen that the calculated effective radius is close to the diffraction-limit prediction. With increasing pulse overlap rate, the accumulated fluence increases and the deviation between the calculated effective radius and the diffraction-limit prediction widens.

After obtaining the effective focal radius, the fluence can be calculated by equation (2) and the thresholds for different pulse overlap rates can be acquired by extending the fitted lines in figure 3 to intersect with the abscissa. Table 1 also lists the ablation thresholds for the three different pulse overlap rates. Clearly, the ablation threshold decreases as the pulse overlap rate increases because of the incubation effect [23].

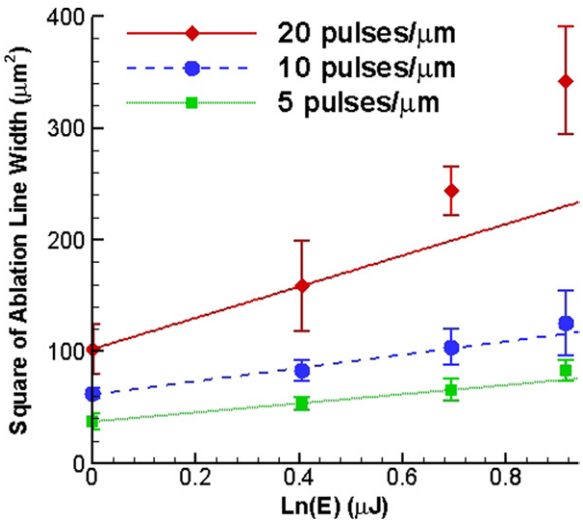

Figure 3. Square of ablation line width versus irradiation pulse energy for the evaluation of effective focal spot size.

Table 1. Effective focal spot radii and ablation thresholds for different pulse overlap rates.

Pulse overlap rate (pulses μm^{-1})	5	10	20
Equivalent pulse number	45	110	336
Effective focal spot radius (μm)	4.5	5.5	8.4
Ablation threshold F_{th} (J cm^{-2})	1.27	0.75	0.43

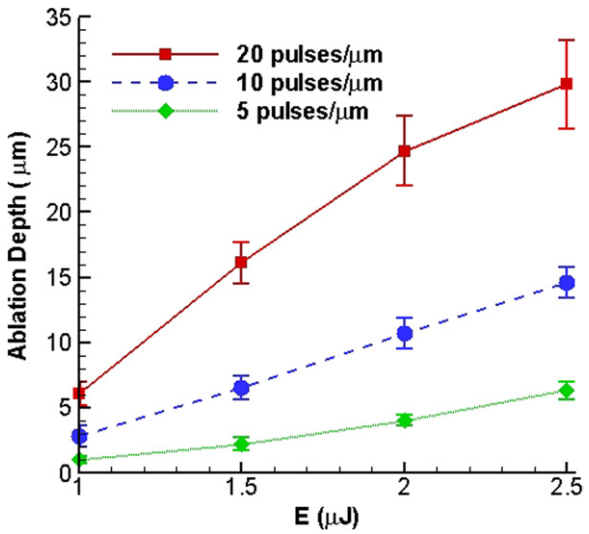

Figure 4. Single line ablation depths as a function of irradiation pulse energy.

An accumulation model is given as

$$F_{\mathrm{th}}(N) = F_{\mathrm{th}}(1)N^{\xi-1}, \tag{4}$$

where $F_{\mathrm{th}}(1)$ and $F_{\mathrm{th}}(N)$ refer to the ablation threshold due to a single pulse and N pulses, respectively. The exponent ξ is the so-called incubation factor. Using the data in table 1, a least-squares fitting line of $\ln(NF_{\mathrm{th}}(N))$ versus $\ln(N)$ can be drawn (not presented here) and the slope yields an incubation factor $\xi = 0.46 \pm 0.03$. Therefore, the ablation threshold for the wet human dermis is determined as $F_{\mathrm{th}}(1) = 9.65 \pm 1.21\,\mathrm{J\,cm^{-2}}$. The uncertainties are obtained using the methods described in [24, 25].

Figure 4 shows the ablation depth changing with the irradiation pulse energy for different pulse overlap rates in the situation of single line scanning ablation. For each ablation depth datum, three samples were measured to obtain the average value and the uncertainty. It should be noticed that in the preparation of fixing and drying for SEM examination, the samples may be somewhat distorted and the distortion affects the measurement accuracy as well. From figure 4 it is seen that the ablation depth increases with both the irradiation pulse energy and the overlap rate. It is known that the pulse overlap rate increases with the pulse repetition rate but decreases with the scanning speed, and the ablation progress is linearly proportional to the scanning speed. For a fixed scanning speed, the ablation production efficiency increases with increasing pulse energy and repetition rate.

3.2. Histological evaluations

In order to examine the degree of thermal damage, the histology of some line scanning ablated samples was analysed. Figure 5 shows the sectional view (200× magnification) of 12 H&E stained wet dermis samples ablated with single line surface scanning with different laser parameters. The selected pulse energies are 1.5 μJ, 2.0 μJ and 2.5 μJ, respectively. The pulse overlap rates are 0.8 pulses $\mu\mathrm{m}^{-1}$, 5 pulses $\mu\mathrm{m}^{-1}$, 10 pulses $\mu\mathrm{m}^{-1}$ and 20 pulses $\mu\mathrm{m}^{-1}$, respectively. The irradiation surface in the pictures faces down and the beam spot is around the middle in each picture. Thermal damaged zone is visualized by the shadow area, because the elastic fibres in the damaged zone are no longer apparent, having been converted into an amorphous, coagulated mass. As observed from figure 5, no thermal damage or structure change occurs in the dermis when the pulse overlap rate is 5 pulses $\mu\mathrm{m}^{-1}$ and below, even in the case of high irradiation pulse energy (2.5 μJ). When the pulse overlap rate is 10 pulses $\mu\mathrm{m}^{-1}$ and above, however, a clear thermal damage zone is observed, in particular when the pulse energy is 2.0 μJ and above. The higher the pulse overlap rate or the higher the pulse energy, the larger and the severer (darker) is the thermal damaged zone. Hence, the accumulation of irradiation fluence is the key factor for causing thermal damage. In order to minimize or eliminate thermal damage, operation with a lower pulse overlap rate is essential. For the cases studied here, a pulse overlap rate up to 5 pulses $\mu\mathrm{m}^{-1}$ is safe for single line ablation.

The study by Suhm *et al* [26] also showed no thermal damage signs in the picosecond laser ablation of neural tissue. Kautek *et al* [27] reported a damage zone of less than 0.5 μm in the ablation of human corneas using a femtosecond pulsed laser. Girard *et al* [28] claimed approximately 14 μm damage zone in the ablation of osseous tissues using a femtosecond Ti : sapphire laser. When long pulsed lasers are utilized, thermal damage zone is more profound. For example, Walsh *et al* [29] found that the damage zone jumped from 50 to 750 μm when the pulse duration increased from 2 μs to 50 ms using CO_2 lasers.

From figure 4 it is obvious that ablation scanning of multiple lines is required in order to achieve practical tissue separation or cutting. Some representative histological results of multi-line ablation are available in figure 6 for evaluation and comparison, where the sectional views (200× magnification) of 16 ablation processed tissue samples with different laser parameters are illuminated. Each tissue sample was repeatedly line scanned for 100 times using experimental setup II. During the processing, the ablation interface was always renewed via the tension through the two opposite tension forces. The selected pulse energies are 1.0 μJ, 1.5 μJ, 2.0 μJ and 2.5 μJ, respectively. The pulse overlap rates are 0.8 pulses $\mu\mathrm{m}^{-1}$, 5 pulses $\mu\mathrm{m}^{-1}$, 10 pulses $\mu\mathrm{m}^{-1}$ and 20 pulses $\mu\mathrm{m}^{-1}$, respectively. The irradiation surface in each picture faces up and the beam focal spot is around the middle. Now clear cuts to a certain depth in all the samples are observed. Comparing figures 5 and 6, the underlying thermal damages in the cases of multi-line ablation are smaller than those in the cases of single line ablation, because the accumulation of the multi-line energy will take away the material in the underlining thermal damage zone. In practical tissue separation or cutting, the underlying damage is not a concern because the tissue has to be cut through.

Table 2 summarizes the sizes of the lateral thermal damage zone around the cut edge for the laser parameter sets considered in figure 6. The thermal damage behaviour for the multi-line scanning cases is very similar to that observed in the single

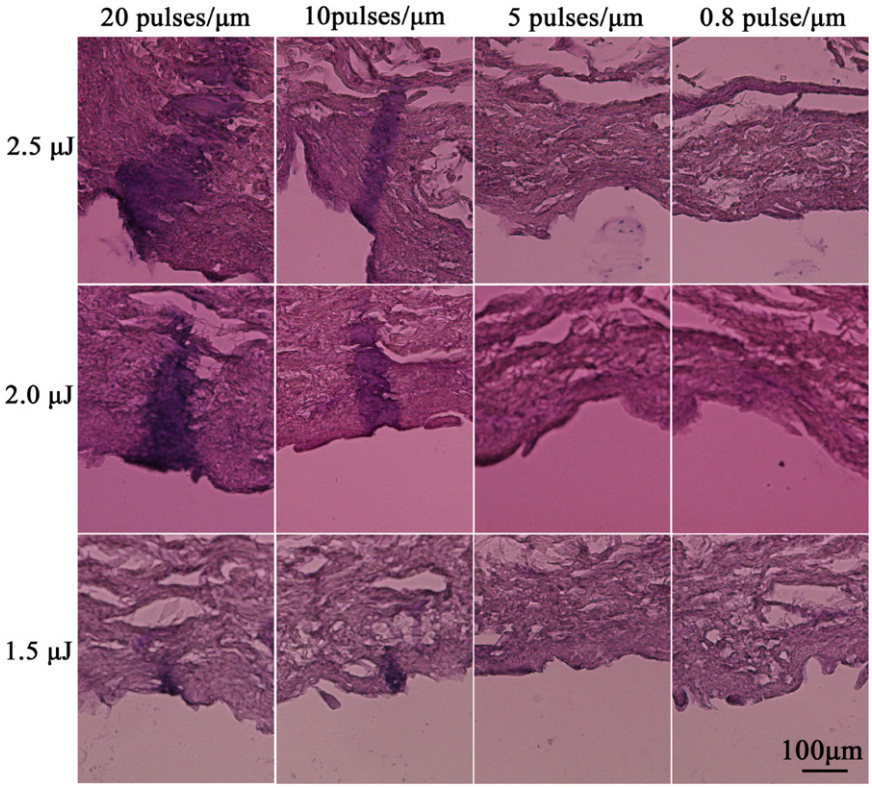

Figure 5. Histological views of single line ablation at wet tissue.

line scanning results, even though the accumulated fluence in multi-line scanning is 100 times stronger than the single line scanning. The reason is that between two successive scans, the lateral accumulation of thermal energy is trivial because the energy has been dissipated into the surroundings. It should be noted that in the cases of 100-line ablation with a pulse overlap rate of 5 pulses μm^{-1}, however, lateral thermal damage is observable within a 10 μm zone when the irradiation pulse energy is 2.0 μJ or above, and the damage is reduced to 2–3 μm when the irradiation pulse energy is below 2.0 μJ. This is because the accumulated energy between two successive scans has not been fully dissipated yet. This problem may be resolved by delaying the repeated scanning time.

Apart from the qualitative examination, figure 6 also shows the cut (ablation) depths for different pulse overlap rates and pulse energies. It is seen that the ablation depth generally increases as the pulse energy and/or overlap rate increase. In the current experiments, two spring steel clips (SBC-78210) were used as the tension forces and the forces were not optimized in line with the single line ablation depth. Thus, the cutting depth due to multi-line ablation is not a simple multiplication of the corresponding single line ablation depth. For example, the 100-line ablation depth for the picture in figure 6 with a pulse overlap rate of 5 pulses μm^{-1} and an irradiation pulse energy of 2.0 μJ is only 210 μm although its single line ablation depth from figure 4 reaches 4.0 μm. Other reasons that could degrade the multi-line ablation depth include beam block by the edges of the prior ablation grooves or by the generated residues and debris and beam alignment. It should also be mentioned that in the preparation of samples for histological view, the samples might be somewhat distorted and this may affect the measurement accuracy as well.

Since the cutting efficiency is directly proportional to the ablation depth and scanning speed, it is desirable to operate the laser tissue processing system at high irradiation pulse energies, high pulse repetition rates and high speeds of scanning. In the same time, the pulse overlap rate must be controlled to avoid thermal damage. In summary, an optimal set of operation parameters for wet dermis cutting and separation is recommended as follows: irradiation pulse energy = 1.5 μJ, stage moving speed = 25 mm s^{-1} (the maximum of the current instrument), pulse repetition rate = 125 kHz and pulse overlap rate = 5 pulses μm^{-1}.

3.3. Tissue separation

The USP laser thin layer separation of wet dermis is demonstrated in figures 7 and 8. Figure 7(*a*) shows an original wet dermis sample before laser ablation. The sample was 30 mm long, 8 mm wide and 1.4 mm thick. Then the tissue was processed with experimental setup II with a pulse overlap rate of 5 pulses μm^{-1} and a pulse energy of 1.5 μJ. Figure 7(*b*) shows the two separated layers that are about 500 μm and 800 μm thick with about 10% unevenness, respectively, for the upper and lower pieces. Both layers are slightly deformed for two reasons: tension forces applied to the tissue during the feeding and pulling process and dehydration of the separated layers due to long-time back and forth motion with the work stage. The separation procedure took about 4 h in the current instrument.

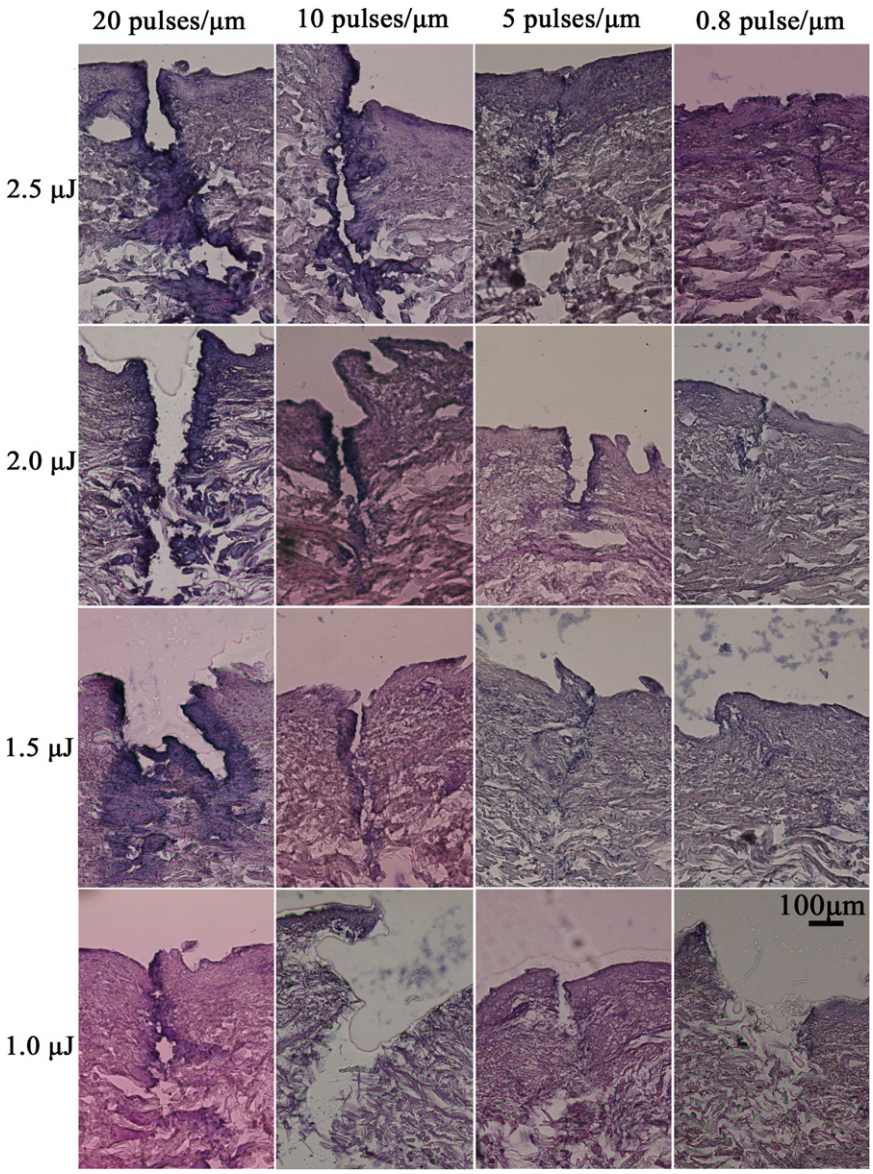

Figure 6. Histological views of multi-line ablation at wet tissue.

Table 2. Lateral thermal damage zones resulting from 100-line ablation.

	f/s			
E (μJ)	20 pulses μm^{-1}	10 pulses μm^{-1}	5 pulses μm^{-1}	0.8 pulse μm^{-1}
2.5	$67 \pm 10\,\mu$m	$40 \pm 8\,\mu$m	$8 \pm 3\,\mu$m	$6 \pm 4\,\mu$m
2.0	$54 \pm 10\,\mu$m	$38 \pm 8\,\mu$m	$6 \pm 4\,\mu$m	$4 \pm 4\,\mu$m
1.5	$52 \pm 8\,\mu$m	$18 \pm 5\,\mu$m	$3 \pm 2\,\mu$m	$3 \pm 3\,\mu$m
1.0	$26 \pm 6\,\mu$m	$3 \pm 2\,\mu$m	$2 \pm 2\,\mu$m	$2 \pm 2\,\mu$m

The separated dermis layers can be further split. Figure 8 shows the partially separated result of another dermis layer of 20 mm long, 6 mm wide and 560 μm thick with the same laser parameters. The thickness of the further separated dermis thin layer is about 220 μm with about 20 μm unevenness. On inspection of the separated layers in figures 7 and 8 no severe thermal damage like charring or melting was found. However, the colour of a part of the separation surface turned to light yellow. Minor lateral thermal damage to the level of about 0.01 mm might have happened in the light yellow region. One big issue is that the current tissue feeding and pulling system is not very precise and optimal. For example, adjustments to keep the tissue moving and addition of water to the moisture chamber were needed during the processing, which may cause unexpected irradiation of the separated edge area. Further improvement of the experimental setup to eliminate the thermal damage and distortion to the separated dermis layer is the future direction. Table 3 lists several dermis tissue separation results

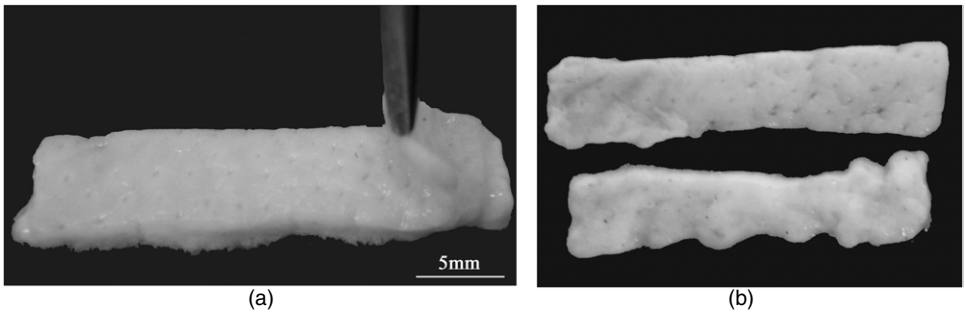

Figure 7. Wet tissue separation by the USP laser ablation: (*a*) the dermis before laser ablation and (*b*) the two separated thin layers.

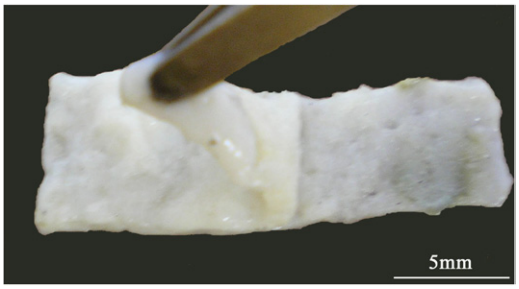

Figure 8. An image of a partially separated dermis.

Table 3. Results from several dermis separation tests.

Sample no	Thickness of the original dermis (mm)	Thickness of the separated thinner layer (mm)
1	0.56	0.22 ± 0.02
2	0.60	0.23 ± 0.02
3	0.80	0.32 ± 0.02
4	0.80	0.33 ± 0.02
5	1.40	0.50 ± 0.03
6	2.00	0.56 ± 0.03

via the current instrument and methodology. The separated layers have a uniform thickness with less than 10% uncertainty.

4. Conclusions

In vitro human dermis separation into thin layers for enhanced usage has been studied via the USP laser ablation for the first time. Several dermis samples are separated into thin layers with thicknesses ranging from 200 to 600 μm. The unevenness of the separated layers is less than 10%. The plasma-mediated ablation mechanism is found to generate less thermal damage to the ablation lines and separation interfaces. The histological evaluations reveal that there is no thermal damage in the single line ablation results when the pulse overlap rate is 5 pulses μm^{-1} and below. In the 100-line repeated ablations, the lateral thermal damage zone is insignificant and generally within 5 μm. In the layer separation with millions of line ablation, the thermal damage is also confined to a small zone of 10 μm. There is no severe thermal damage like charring or melting existing in the multi-line ablation and layer separation results. The slight thermal damage is caused by the current crude device for tissue feeding and pulling during laser processing. Design and fabrication of a precise work stage is required in future studies.

The fundamental ablation features of a wet dermis are investigated. The ablation threshold for the dermal tissue is found to be 9.65 ± 1.21 J cm^{-2}. The accumulation effect is very obvious in dermis ablation and its incubation factor is found to be 0.46. The rough surface of the dermis leads to strong scattering of light at the surface. When the pulse overlap rate is 5 pulses μm^{-1}, the calculated effective spot radius is about 15% larger than the diffraction-limit prediction. With a further increase in the pulse overlap rate, the accumulated fluence increases and the deviation between the calculated effective radius and the diffraction-limit prediction widens. The ablation width and depth increase as the pulse energy and/or overlap rate increase. In terms of cutting efficiency, it is desirable to operate the laser tissue processing system at high irradiation pulse energies, high pulse repetition rates and high speeds of scanning. At the same time, the pulse overlap rate must be controlled to avoid thermal damage. There exists a trade-off of balance between the productivity and the minimization of thermal damage.

Acknowledgments

This work was supported by the Musculoskeletal Transplant Foundation (MTF). The authors are grateful to Michael Schuler and Arthur Gertzman at MTF for their help and constructive comments, to Alex Scozzarro at MTF for preparing and providing dermis samples, to Greg Spooner at Raydiance, Inc., for providing technical support and to Tin O Khor and Siwang Yu at Rutgers University for assisting with the histological examinations.

References

[1] Schuler M and Gertzman A 2007 private communication
[2] Kearney J N 2005 Guidelines on processing and clinical use of skin allografts *Clin. Dermatol.* **23** 357–64
[3] Costantino P D, Govindaraj S, Hiltzik D H, Buchbinder D and Urken M L 2001 Acellular dermis for facial soft tissue augmentation preliminary report *Arch. Facial Plast. Surg.* **3** 38–43
[4] Spear S L, Parikh P M, Reisin E and Menon N G 2008 Acellular dermis-assisted breast reconstruction *Aesth. Plast. Surg.* **32** 418–25
[5] Buck B E and Malinin T I 1994 Human bone and tissue allografts. Preparation and safety *Clin. Orthop. Relat. Res.* **303** 8–17

[6] Niemz M H 2003 *Laser–Tissue Interactions: Fundamentals and Applications* 3rd edn (Heidelberg: Springer)
[7] Guo Z, Wan S K, August D A, Ying J, Dunn S M and Semmlow J L 2006 Optical imaging of breast tumor through temporal log-slope difference mappings *Comput. Biol. Med.* **36** 209–23
[8] Niemz M H, Klancnik E G and Bille J F 1991 Plasma-mediated ablation of corneal tissue at 1053 nm using a Nd : YLF oscillator/regenerative amplifier laser *Lasers Surg. Med.* **11** 426–31
[9] Fischer J P, Dams J, Götz M H, Kerker E, Loesel F H, Messer C J, Suhm N, Niemz M H and Bille J F 1993 Plasma-mediated ablation of brain tissue with picosecond laser pulses *Appl. Phys.* B **58** 493–9
[10] Moss J P, Patel B C, Pearson G J, Arthur G and Lawes R A 1994 Krypton fluoride excimer-laser ablation of tooth tissues: precision tissue machining *Biomaterials* **15** 1013–8
[11] Loesel F H, Fischer J P, Götz M H, Horvath C, Juhasz T, Noack F, Suhm N and Bille J F 1998 Non-thermal ablation of neural tissue with femtosecond laser pulses *Appl. Phys.* B **66** 121–8
[12] Chen S C, Kancharla V and Lu Y 2003 Laser-based microscale patterning of biodegradable polymers for biomedical applications *Int. J. Mater. Prod. Technol.* **18** 457–68
[13] Aguilar C A, Lu Y, Mao S and Chen S 2005 Direct micro-patterning of biodegradable polymers using ultraviolet and femtosecond lasers *Biomaterials* **26** 7642–49
[14] Huang H and Guo Z 2009 Ultra-short pulsed laser PDMS thin-layer separation and micro-fabrication *J. Micromech. Microeng.* **19** 055007
[15] Liu Y M, Sun S, Singha S, Cho M R and Gordon R J 2005 3D femtosecond laser patterning of collagen for directed cell attachment *Biomaterials* **26** 4597–605
[16] Hallgren C, Reimers H, Chakarov D, Gold J and Wennerberg A 2003 An *in vivo* study of bone response to implants topographically modified by laser micromachining *Biomaterials* **24** 701–10
[17] Troy T L and Thennadil S N 2001 Optical properties of human skin in the near infrared wavelength range of 1000 to 2200 nm *J. Biomed. Opt.* **6** 167–76
[18] Spooner G J 2007 private communication
[19] Baudach S, Bonse J and Kautek W 1999 Ablation experiments on polyimide with femtosecond laser pulses *Appl. Phys.* A **69** S395–8
[20] Bonse J, Wrobel J M, Krüger J and Kautek W 2001 Ultrashort-pulse laser ablation of indium phosphide in air *Appl. Phys.* A **72** 89–94
[21] Mullan C, O'Connor G M, Favre S, Ilie D and Glynn T J 2007 Estimating spot size and relating hole diameters with fluence and number of shots for nanosecond and femtosecond laser ablation of polyethylene terephthalate *J. Laser Appl.* **19** 158–64
[22] Choi H W, Johnson J K, Nam J, Farson D F and Lannutti J 2007 Structuring electrospun polycaprolactone nanofiber tissue scaffolds by femtosecond laser ablation *J. Laser Appl.* **19** 225–31
[23] Rosenfeld A, Lorenz M, Stoian R and Ashkenasi D 1999 Ultrashort laser pulse damage threshold of transparent materials and the role of incubation *Appl. Phys.* A **69** S373–6
[24] Higbie J 1991 Uncertainty in the linear regression slope *Am. J. Phys.* **59** 184–5
[25] Holman J P 2001 *Experimental Methods for Engineers* 7th edn (Boston: McGraw-Hill)
[26] Suhm N, Götz M H, Fischer J P, Loesel F, Schelgel W, Sturm V, Bille J and Schröder R 1996 Ablation of neural tissue by short pulsed laser: a technical report *Acta Neurochir.* **138** 346–9
[27] Kautek W, Mitterer S, Krüger J, Husinsky W and Grabner G 1994 Femtosecond-pulse laser ablation of human corneas *Appl. Phys.* A **58** 513–8
[28] Girard B, Yu D, Armstrong M R, Wilson B C, Clokie C M L and Miller R J D 2007 Effects of femtosecond laser irradiation on osseous tissues *Lasers Surg. Med.* **39** 273–85
[29] Walsh J T Jr, Flotte T J, Anderson R R and Deutsch T F 1988 Pulsed CO_2 laser tissue ablation: effect of tissue type and pulse duration on thermal damage *Lasers Surg. Med.* **8** 108–18